FlashMem: Distilling Intrinsic Latent Memory via Computation Reuse

Yubo Hou[1], Zhisheng Chen[2,3], Tao Wan[4], Zengchang Qin[1,5]*
[1]School of ASEE, Beihang University, Beijing, China
[2]Institute of Computing Technology, Chinese Academy of Sciences, Beijing, China
[3]University of Chinese Academy of Sciences, Beijing, China
[4]School of BME, Beijing Advanced Innovation Center for BME, Beihang University
[5]CAIR and CECS, VinUniversity, Hanoi, Vietnam
houyubo@buaa.edu.cn, *zengchang.qin@gmail.com

Abstract

The stateless architecture of Large Language Models inherently lacks the mechanism to preserve dynamic context, compelling agents to redundantly reprocess history to maintain long-horizon autonomy. While latent memory offers a solution, current approaches are hindered by architectural segregation, relying on auxiliary encoders that decouple memory from the reasoning backbone. We propose **FlashMem**, a framework that distills intrinsic memory directly from transient reasoning states via computation reuse. Motivated by prior findings that final-layer representations preserve rich information about the input trajectory, FlashMem uses the last hidden state as a compact and empirically effective summary of the interaction history. This enables a **Shared-KV Consolidator** to synthesize memory by attending directly to the backbone's frozen cache, eliminating redundant re-parameterization. Furthermore, a parameter-free **Cognitive Monitor** leverages attention entropy to adaptively trigger consolidation only when high epistemic uncertainty is detected. Experiments demonstrate that FlashMem matches the performance of heavy baselines while reducing inference latency by **5 times**, effectively bridging the gap between efficiency and persistent cognition.

1 Introduction

The capability to sustain coherent epistemic states across extended temporal horizons is a prerequisite for general-purpose autonomy. While Large Language Models (LLMs) function as powerful reasoning engines, their architecture is fundamentally stateless: they map inputs to outputs based on static parameters without retaining a persistent internal state between interactions. This design creates a dichotomy between the model's frozen parametric knowledge and the dynamic procedural context required for long-horizon tasks. Consequently, in evolving workflows, agents are forced to discard rich intermediate reasoning representations after every inference step (Hu et al., 2026). This statelessness necessitates the redundant reprocessing of historical information, creating a significant bottleneck for agents that must continually accumulate experience and adapt.

To eliminate the gap between transient inference and persistent cognition, memory mechanisms have become a focal point of research. Current approaches are generally categorized into parametric, token-level, and latent forms (Hu et al., 2026). Parametric updates are computationally prohibitive for real-time adaptation, while token-level retrieval (e.g., Mem0 (Chhikara et al., 2025)) often suffers from low information density, crowding out the finite context window with raw text rather than synthesized understanding. Addressing these limitations, Generative Latent Memory has emerged as a promising paradigm (Zhang et al., 2025; Xu et al., 2025a). By compressing broad contexts into dense continuous vectors, these methods function as compact cognitive buffers, preserving critical information without exhausting attention budgets.

However, a structural inefficiency persists in state-of-the-art latent memory paradigms due to *architectural segregation* and *computational redundancy*. Prevalent methods typically synthesize memory via parameter-divergent auxiliary modules—whether independent encoders (Wu et al., 2025; Yu et al., 2025) or specialized adapters (Zhang et al., 2025)—that are detached from the primary reasoning backbone. This bifurcation prevents the direct reuse of the backbone's cached Key-Value (KV) states, compelling the system to maintain disjoint memory buffers and perform duplicate forward passes for context re-encoding. Furthermore, relying on iterative optimization (Li et al., 2025a) or full-scale autoregressive decoding for memory generation inevitably interrupts the continuous flow of thought, introducing

*Corresponding author.

Findings of the Association for Computational Linguistics: ACL 2026, pages 4687–4705

substantial inference latency. We argue that an efficient memory mechanism should instead be *intrinsic*—harvesting memory directly from the agent's existing computational flow to bypass redundant re-parameterization.

Realizing this vision, we propose **FlashMem**, a framework that distills latent memory directly from the agent's transient reasoning states via computation reuse. Motivated by prior analyses suggesting that LLM final-layer representations retain rich trajectory information (Nikolaou et al., 2025), FlashMem uses the last hidden state as a compact summary of the interaction history and as the seed for memory synthesis. This allows us to employ a **Shared-KV Consolidator** that synthesizes memory by attending directly to the backbone's frozen cache, effectively treating the reasoning process itself as the definitive source of memory without structural segregation. Complementing this, to align memory generation with real-time epistemic needs, we introduce a parameter-free **Cognitive Monitor**. Grounded in the correlation between attention entropy and model uncertainty (Kuhn et al., 2023; Farquhar et al., 2024), this mechanism triggers consolidation exclusively when the agent exhibits high internal confusion.

Our contributions are summarized as follows:

- We propose **FlashMem**, a lightweight framework designed to distill intrinsic memory via *computation reuse*. Unlike segregated architectures that require heavy re-encoding, FlashMem directly harvests the backbone's transient reasoning states, offering a high-efficiency solution for long-horizon agents without architectural decoupling.
- We develop a minimalist **Shared-KV Consolidator** motivated by the observation that the last hidden state provides a compact summary for memory synthesis. By synthesizing memory directly from the backbone's frozen cache, this design eliminates redundancy. Empirical results demonstrate that it achieves performance parity with heavy baselines while reducing inference latency by **5**$\times$ with negligible VRAM overhead.
- We introduce a parameter-free **Cognitive Monitor** that utilizes attention entropy as a real-time signal for epistemic uncertainty. Our analysis demonstrates that high entropy effectively localizes model confusion and hallucinations, enabling the monitor to adaptively trigger memory consolidation only when necessary to prevent wasteful computation.

2 Related Work

Recent scholarship classifies agent memory into *token-level*, *parametric*, and *latent* forms (Hu et al., 2026). While each has advanced the field, structural inefficiencies persist in how they are generated and managed.

Token-level and Parametric Memory. Token-level memory (e.g., RAG (Lewis et al., 2020), MemGPT (Packer et al., 2024), Mem0 (Chhikara et al., 2025)) offers transparency but suffers from low information density, often exhausting finite attention budgets with retrieved context. Conversely, parametric memory (e.g., ROME (Meng et al., 2022)) provides inference efficiency by internalizing knowledge into weights but lacks the plasticity required for real-time, intra-episode adaptation (Hu et al., 2026).

Generative Latent Memory. To improve density, research has shifted towards active memory generation, encoding context into continuous vectors. Prominent works such as MemGen (Zhang et al., 2025) and SoftCoT (Xu et al., 2025a) employ auxiliary modules—independent encoders or distinct LoRA adapters—to compress context into gist tokens (Mu et al., 2023) or latent states. Multimodal extensions like VisMem (Yu et al., 2025) and CoMEM (Wu et al., 2025) similarly rely on separate encoders. However, these architectures are computationally heavy. For instance, MemGen necessitates maintaining three distinct model instances (Trigger, Weaver, and Reasoner) concurrently, while SoftCoT relies on autoregressive decoding or iterative optimization to synthesize prompts. Consequently, they necessitate re-encoding history through secondary parameters, causing significant redundancy and VRAM overhead. MemOS (Li et al., 2025b) is also related in its reuse of cached activations, but it focuses on reusable memory management rather than online synthesis of interaction-specific memory.

Efficiency and Cognitive Control. To mitigate the high costs of long-context reasoning, research focuses on two optimization paths: state compression and selective activation. Heuristic methods like SnapKV (Li et al., 2024), H2O (Zhang et al.,

2023), and PyramidKV (Cai et al., 2025) compress the KV cache by pruning less attentive tokens. While fast, these extractive approaches risk severing long-range semantic dependencies compared to generative synthesis. Beyond compression, optimizing activation timing is equally critical. Existing systems often rely on static prompts or heavy trainable classifiers (Zhang et al., 2025), ignoring the established link between attention entropy and model uncertainty (Kuhn et al., 2023; Farquhar et al., 2024; Guerreiro et al., 2023). FlashMem addresses these limitations by integrating a Shared-KV consolidator for efficient computation reuse and a parameter-free entropy monitor for self-regulated activation.

3 Methodology

3.1 Preliminaries and Problem Formulation

Agent Formulation and the Efficiency Gap. We formalize an LLM-based agent as a parametric policy π_θ interacting via a trajectory $\tau_{<t} = (o_1, a_1, \ldots, o_{t-1}, a_{t-1})$. At step t, the agent samples action a_t conditioned on the history $\tau_{<t}$, current observation o_t, and auxiliary memory $\mathcal{M}$:

$$a_t \sim \pi_\theta(\cdot \mid \tau_{<t}, o_t, \mathcal{M}) \tag{1}$$

In this work, we focus on *Latent Memory*, represented as continuous embeddings $\mathcal{M} = \{m_1, \ldots, m_K\}$ ($m_i \in \mathbb{R}^d$). Unlike token-level retrieval, latent memory functions as a high-density buffer that encodes abstract reasoning patterns with minimal token overhead.

However, prevalent paradigms typically adopt a segregated architecture, generating memory via an auxiliary process $\mathcal{G}_\phi$:

$$\mathcal{M} = \mathcal{G}_\phi(\tau_{<t}) \tag{2}$$

This necessitates an independent encoding pass, incurring *computational redundancy* via the repetitive encoding of $\tau_{<t}$ and *state segregation* due to the maintenance of disjoint KV caches. Our goal is to synthesize $\mathcal{M}$ intrinsically by reusing the backbone's states.

3.2 Overview of FlashMem

To address the aforementioned efficiency gaps, we introduce **FlashMem**, a memory generation architecture that is deeply coupled with the LLM backbone π_θ. As illustrated in Figure 1, unlike segregated systems that rely on independent encoding passes, FlashMem operates on the principle of computation reuse: it synthesizes memory directly from the backbone's transient activation states, thereby eliminating repetitive encoding and the overhead of maintaining disjoint KV caches. The framework comprises two synergistic components:

- **The Cognitive Monitor (Sec. 3.3):** A parameter-free gating mechanism that determines *when* to generate memory. Upon detecting high entropy (signaling model confusion), the monitor suspends standard generation to initiate memory consolidation.
- **The Memory Consolidator (Sec. 3.4):** A lightweight decoder designed to determine *how* to synthesize memory efficiently. To avoid re-processing the long historical trajectory, it adopts a shared-KV design. Specifically, it projects the backbone's current hidden state h_t to serve as the initial query, and then attends directly to the backbone's accumulated KV cache. This mechanism enables FlashMem to distill valuable knowledge and experiential patterns directly from the backbone's high-level representations, bypassing the need for redundant re-encoding.

Inference Workflow. During inference, FlashMem dynamically switches between standard generation and memory-augmented modes. The synthesized memory $\mathcal{M}$ is soft-injected back into the backbone's input stream. These latent embeddings serve as high-density cognitive cues, not only surfacing relevant historical context but also injecting abstract reasoning patterns to steer subsequent complex decision-making.

3.3 The Cognitive Monitor: Entropy-Based Uncertainty Perception

Current generative memory paradigms often rely on rigid triggering mechanisms: either static injection—exemplified by SoftCoT (Xu et al., 2025a) which indiscriminately prepends tokens—wasting computation on simple queries, or learned classifiers like MemGen (Zhang et al., 2025), which introduce architectural overhead and distribution shift risks. Instead, we propose to leverage the LLM's intrinsic uncertainty as a parameter-free activation signal. Pioneering works in uncertainty estimation (Kuhn et al., 2023) and hallucination detection (Farquhar et al., 2024) have established that the dispersion of a model's internal probability

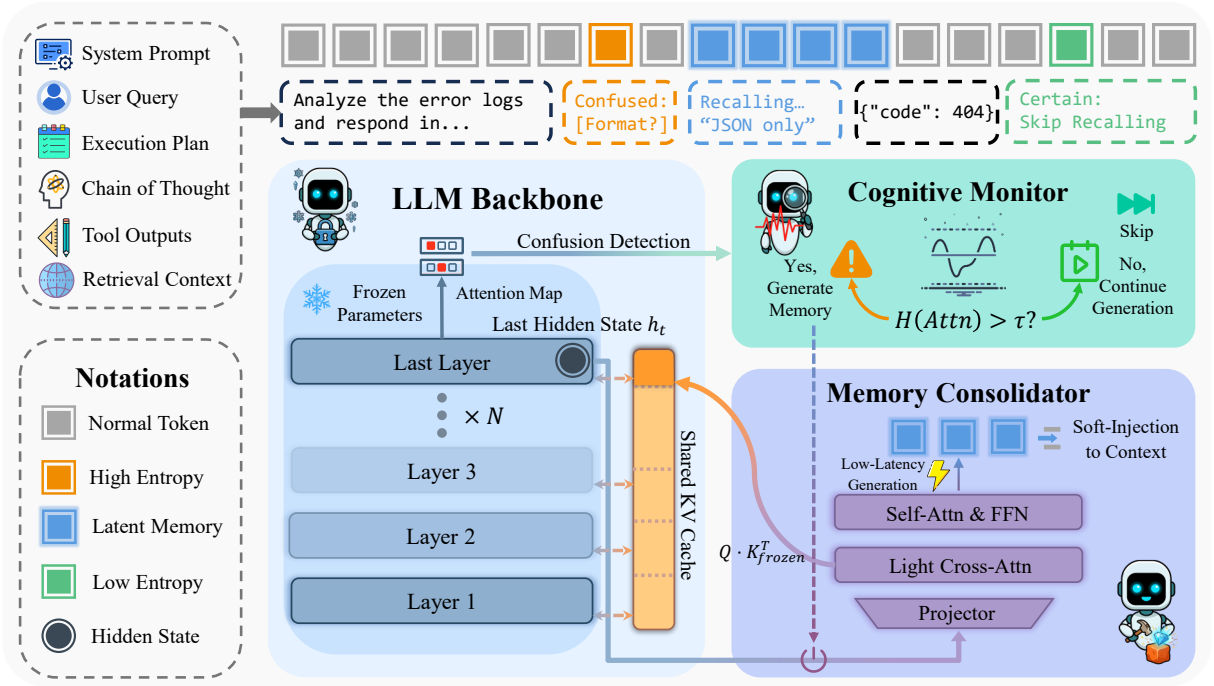

Figure 1: The architecture of **FlashMem**. It features a parameter-free **Cognitive Monitor** (top right) that activates memory generation based on attention entropy uncertainty, and a lightweight **Memory Consolidator** (bottom right). The consolidator utilizes a *Shared-KV* design to efficiently generate latent memories by reusing the frozen backbone's cache, taking the hidden state h_t as the initiation seed.

distribution correlates strongly with its semantic confidence. Specifically, when a model is confused or prone to confabulation, its attention mechanism tends to exhibit high entropy, lacking focus on salient tokens (Guerreiro et al., 2023). Building on this theoretical consensus, we employ attention entropy as a real-time metacognitive indicator.

Mitigating Attention Sinks. However, calculating entropy directly from raw attention weights is unreliable due to the *attention sink* phenomenon (Xiao et al., 2024). Studies show that LLMs (and Vision Transformers (Darcet et al., 2024)) notoriously allocate massive attention scores to initial tokens (e.g., [BOS]), regardless of their semantic irrelevance. This dominant sink artificially acts as a low-entropy anchor, masking the true dispersion of the reasoning process. To extract a de-noised cognitive signal, we process the attention weights from the last layer, which has been shown to encode the most semantic-rich and task-specific information (Tenney et al., 2019). Let $A_{t,h} \in \mathbb{R}^t$ denote the attention distribution of head h at the current step t over the context sequence. We define $\mathcal{S}_{\text{sink}}$ as the set of indices corresponding to the attention sinks. We explicitly mask these tokens and re-normalize the distribution for each head:

$$\tilde{A}_{t,h}[j] = \frac{A_{t,h}[j] \cdot \mathbb{I}(j \notin \mathcal{S}_{\text{sink}})}{\sum_k A_{t,h}[k] \cdot \mathbb{I}(k \notin \mathcal{S}_{\text{sink}})} \quad (3)$$

where $\mathbb{I}$ is the indicator function and j, k represent token indices.

Entropy Decision and Adaptive Intervention. We calculate the Shannon entropy for each head individually to capture diverse uncertainty patterns, and then aggregate them to form the final metric. The system uncertainty $\mathcal{H}_t$ is defined as the average entropy across all H heads:

$$\mathcal{H}_t = \frac{1}{H} \sum_{h=1}^{H} \left(- \sum_{j \notin \mathcal{S}_{\text{sink}}} \tilde{A}_{t,h}[j] \log \tilde{A}_{t,h}[j] \right) \quad (4)$$

Memory consolidation is activated only when $\mathcal{H}_t > \tau$. The threshold τ functions as a sensitivity knob governing the efficiency-performance trade-off. A lower τ encourages the agent to seek memory aid more aggressively (prioritizing accuracy), while a higher τ restricts intervention to moments of severe confusion (prioritizing speed). This flexibility allows FlashMem to adapt to varying computational budgets at test time, offering a distinct advantage over fixed-cost classifiers. In practice,

rather than relying on a fixed heuristic value, we adopt a distribution-aware calibration strategy. The optimal baseline for τ correlates with the model's intrinsic confidence and the task's open-endedness. We discuss these entropy dynamics and detail our statistical calibration protocol in Appendix D.

3.4 The Memory Consolidator: Shared-KV Generation

Upon activation, the system aims to synthesize memory efficiently. To achieve this, we introduce the **Memory Consolidator**, a lightweight decoder architecture designed strictly around the principle of computation reuse.

State Projection from Final-Layer Representations. Motivated by prior work showing that final-layer representations preserve substantial information about the input trajectory (Nikolaou et al., 2025), we use the backbone's last hidden state h_t as a compact semantic summary of the preceding context. Instead of re-encoding inputs, we treat the backbone as a pre-computed encoder. We project h_t into the consolidator's working dimension via a two-layer MLP to produce the initial latent embedding m_0. This allows the Consolidator to inherit the backbone's comprehension without redundant processing.

Projection-Free Cross-Attention. The Consolidator consists of L stacked decoder layers. To minimize parameter count and VRAM usage, we introduce a projection-free cross-attention mechanism. Unlike standard attention layers that require trainable projections for Keys and Values, we discard W_K and W_V. Let x denote the input state to the current layer, initialized as m_0. The module computes only the Query vector using x and attends directly to the backbone's accumulated key and value matrices $\mathbf{K}$ and $\mathbf{V}$:

$$\text{Attn}(x, \mathbf{K}, \mathbf{V}) = \text{softmax}\left(\frac{(xW_Q)\mathbf{K}^\top}{\sqrt{d}}\right)\mathbf{V} \quad (5)$$

where W_Q is the only learnable projection matrix in the attention operation. This mechanism ensures negligible storage overhead for context maintenance, as the generation process is anchored to the backbone's existing state pool.

Weight Inheritance and Soft Injection. Training a lightweight module from scratch to collaborate with a frozen, massive backbone presents a significant semantic alignment challenge. Random initialization often results in a large distributional shift, leading to unstable optimization. To mitigate this, we employ a homologous weight inheritance strategy. Specifically, we initialize the Consolidator's parameters using the last L layers of the backbone, where $L \ll N_{backbone}$. This initialization places the Consolidator within a semantic manifold compatible with the backbone from the start, significantly accelerating convergence and facilitating smoother representation alignment. The Consolidator then auto-regressively generates K latent embeddings $\mathcal{M} = \{m_1, \ldots, m_K\}$, which are soft-injected into the backbone's input stream to guide subsequent reasoning.

4 Experiments

4.1 Experimental Setup

We evaluate FlashMem on six benchmarks: reasoning (GSM8K (Cobbe et al., 2021), MATH (Hendrycks et al., 2021), GPQA (Rein et al., 2023)), coding (KodCode (Xu et al., 2025b)), and summarization (BookSum (Kryscinski et al., 2022), GovReport (Huang et al., 2021)). We compare against three paradigms: (1) direct generation (Vanilla, CoT-SC (Wang et al., 2023)); (2) KV compression (SnapKV (Li et al., 2024)); and (3) generative latent memory (MemGen (Zhang et al., 2025)). Experiments utilize instruct-tuned backbones from Qwen (2.5-1.5B, 3-4B) (Yang et al., 2024, 2025) and Llama (3.1-8B, 3.2-3B) (Meta, 2024a,b). A lightweight Consolidator is trained via SFT for each backbone while keeping the backbone frozen; detailed protocols and hyperparameters are in Appendix A. Appendix B also reports results on Qwen3-14B/32B, additional baselines (SoftCoT, LatentSeek, and MemOS), LongBench v2 (Bai et al., 2024) and RULER, and matched SFT controls.

4.2 Main Results

Tables 1 and 2 present the performance of FlashMem against baselines on the Qwen and Llama families, respectively.

Competitive Reasoning Fidelity. FlashMem achieves parity with the heavy-weight MemGen baseline across reasoning tasks without relying on independent encoders. For instance, on Qwen 2.5 (Table 1), FlashMem reaches **70.09%** on GSM8K, closely trailing MemGen (70.54%) while significantly outperforming the Vanilla baseline. Notably, on the smaller Llama 3.2 3B model (Table 2),

Table 1: **Results on Qwen Family.** We compare FlashMem with baselines on Qwen 2.5 (1.5B) and the latest Qwen 3 (4B). Metric: Accuracy (%) for Reasoning/Code, ROUGE-1 for Summarization. FlashMem consistently matches or exceeds the segregated latent memory baseline (MemGen) while maintaining superior efficiency. Best results are **bolded**, and second-best results are underlined.

Dataset	Metric	Qwen 2.5 1.5B Instruct					Qwen 3 4B Instruct				
		Vanilla	CoT-SC	SnapKV	MemGen	FlashMem	Vanilla	CoT-SC	SnapKV	MemGen	FlashMem
Mathematical & Scientific Reasoning											
GSM8K	ACC	65.12	68.98	54.37	**70.54**	70.09	80.49	82.65	69.88	**85.42**	84.38
MATH	ACC	40.71	43.77	38.00	46.55	**50.16**	54.22	54.96	50.12	**60.23**	58.36
GPQA	ACC	13.96	15.14	13.66	**16.13**	14.73	16.84	17.95	14.54	**21.68**	20.54
Code Generation											
KodCode	ACC	22.85	29.30	39.70	**55.70**	50.20	56.48	57.55	49.70	59.77	**61.13**
Long-Context Summarization											
BookSum	R-1	11.14	11.62	10.38	12.86	**13.77**	8.93	9.35	**11.12**	10.18	10.99
GovReport	R-1	13.61	14.41	14.22	13.97	**16.11**	13.65	13.87	13.74	14.31	**15.52**

Table 2: **Results on Llama Family.** Performance comparison on Llama 3.1 (8B) and Llama 3.2 (3B). FlashMem demonstrates robust generalization across different parameter scales, particularly excelling in summarization and code tasks on smaller architectures. Best results are **bolded**, and second-best results are underlined.

Dataset	Metric	Llama 3.1 8B Instruct					Llama 3.2 3B Instruct				
		Vanilla	CoT-SC	SnapKV	MemGen	FlashMem	Vanilla	CoT-SC	SnapKV	MemGen	FlashMem
Mathematical & Scientific Reasoning											
GSM8K	ACC	68.38	68.91	57.30	**71.12**	70.46	60.48	60.76	55.62	**63.68**	62.35
MATH	ACC	45.97	50.37	44.23	50.95	**51.56**	40.77	44.12	37.14	45.17	**48.05**
GPQA	ACC	15.48	17.80	15.66	**18.43**	17.86	4.79	5.18	5.27	**7.07**	6.70
Code Generation											
KodCode	ACC	34.61	37.90	40.88	**57.70**	54.27	21.93	26.27	20.33	29.64	**29.98**
Long-Context Summarization											
BookSum	R-1	13.12	14.62	11.67	**15.61**	14.65	9.03	9.29	10.25	**12.09**	11.04
GovReport	R-1	13.95	15.41	12.81	16.37	**17.23**	12.92	13.61	14.43	13.44	**14.55**

FlashMem even surpasses MemGen on the challenging MATH dataset (**48.05%** vs. 45.17%), suggesting that the shared-KV design may better preserve mathematical priors in smaller parametric spaces.

Long-Context Superiority and Robustness. FlashMem exhibits particular strength in summarization and structure-heavy tasks, consistently outperforming MemGen on GovReport and KodCode across most backbones. On the Qwen 3 4B model, FlashMem leads on both KodCode (**61.13%**) and GovReport (**15.52%**), indicating that deriving memory directly from the backbone's high-fidelity KV cache captures global semantics better than re-encoding the history. Furthermore, FlashMem significantly outperforms the KV compression baseline SnapKV (e.g., a **+11%** gap on Qwen 3 KodCode), confirming that generative latent memory is essential for preserving the complex dependencies that heuristic pruning methods typically discard.

Broader Evaluation. This trend persists in the additional evaluations. On Qwen3-14B/32B, FlashMem remains close to MemGen on reasoning and improves on KodCode and GovReport, reaching 70.91 and 29.31, respectively, with Qwen3-32B. On Qwen3-4B, it also outperforms SoftCoT and LatentSeek on KodCode and GovReport while keeping much lower 64k latency. FlashMem further reaches 41.5 on LongBench v2 and 88.5 / 97.2 on RULER-64k NIAH / multi-hop tracing. Appendix B reports the full results.

MemOS and Matched SFT Controls. We also compare FlashMem with MemOS and matched SFT baselines. FlashMem is stronger than MemOS (Li et al., 2025b) on KodCode and GovReport, and is also more efficient in the compared 64k setting. Under the same expert trajectories, it outperforms both Full SFT and one-layer LoRA SFT on KodCode, suggesting that supervision alone

does not account for the gain. Appendix B provides the detailed comparison.

4.3 Efficiency Analysis

To empirically validate the architectural efficiency of FlashMem, we conducted a stress test focusing on computational latency and memory footprint under long-context conditions.

Benchmark Protocol. We implemented a *cyclic generation benchmark* on a single NVIDIA A100-80GB GPU. The evaluation follows an iterative pattern of 8 cycles where the model generates 32 text tokens followed by 8 latent memory tokens. We scaled the input context length L from 4,096 (4k) to 65,536 (64k) tokens across Vanilla, MemGen (Zhang et al., 2025), and FlashMem configurations.

Efficiency Results. As shown in Table 3, the segregated architecture of MemGen exhibits poor scalability: at 64k tokens, its VRAM usage rises to **40.78 GB** (nearly 10 GB overhead), while effective throughput collapses to **4.13 tokens/s** due to re-encoding bottlenecks. In contrast, FlashMem maintains a highly efficient profile nearly identical to the Vanilla baseline (31.44 GB vs 31.21 GB VRAM) while sustaining robust throughput (20.86 tokens/s). Crucially, in terms of latency per step at maximum context, FlashMem (**12.28 ms**) achieves an approximate $\mathbf{5}\times$ speedup over MemGen (61.99 ms), confirming that the shared-KV design effectively eliminates redundant storage and computation.

4.4 Impact of Consolidator Depth

To determine the optimal configuration for the Memory Consolidator, we investigated the effect of layer depth L ($1 \leq L \leq 6$) on both reasoning performance and computational cost.

Performance Saturation. Table 4 details the accuracy on GSM8K and KodCode. We observe immediate performance saturation: the single-layer model ($L = 1$) achieves 69.55% on GSM8K, which is comparable to deeper configurations. Similarly, on the structure-sensitive KodCode task, increasing depth from $L = 1$ to $L = 6$ yields negligible gains (e.g., 50.10% vs. 50.29%). This empirical evidence strongly suggests that a single-layer Consolidator is sufficient to distill high-quality latent memory from the backbone's shared KV cache, validating our minimalist design philosophy.

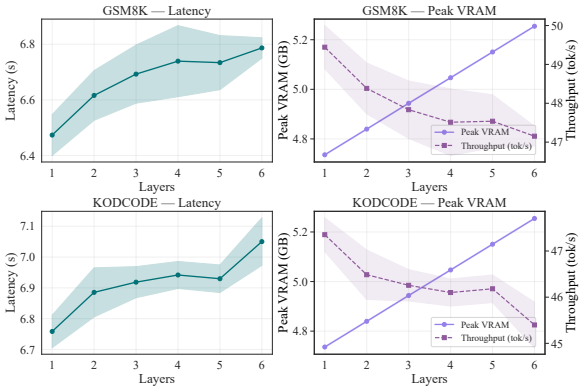

Figure 2: **Efficiency Trade-offs across Layer Depths.** VRAM usage scales linearly with depth, while latency increases monotonically. Combined with Table 4, results favor a minimal depth configuration.

Cost Analysis. While accuracy plateaus, the computational overhead increases with depth. As illustrated in Figure 2, VRAM usage exhibits a strict linear growth, directly correlating with the increase in parameters. In contrast, inference latency shows a monotonic increase (and throughput a corresponding decrease), reflecting the accumulated overhead of sequential decoding. Given that $L = 1$ offers nearly identical reasoning support with the lowest resource footprint, we conclude that shallow architectures are optimal for the FlashMem framework.

5 Mechanism Analysis

5.1 Effectiveness of Cognitive Monitor

We hypothesize that the *Cognitive Monitor* acts as an uncertainty detector, identifying critical decision points where the model lacks internal knowledge. To validate this, we analyzed inference traces on the GSM8K dataset, specifically focusing on samples where the Vanilla model failed while FlashMem succeeded.

Qualitative Analysis: Entropy Dynamics. Figure 3 illustrates the attention entropy trajectories across four different backbones. In these cases, the Vanilla baseline exhibits sustained or rising entropy at critical reasoning steps, indicative of cognitive confusion that eventually leads to logical errors. In contrast, FlashMem successfully identifies these high-entropy peaks. Upon injecting the synthesized latent memory, we observe a pronounced reduction in attention entropy, reflecting a significant decrease in the model's internal uncertainty in subsequent tokens. This confirms that the Cognitive Monitor effectively pinpoints

Table 3: **Efficiency Benchmark on Long-Context Inference.** We report the **Peak VRAM** usage (maximum observed), along with **Effective Generation Throughput** (excluding latent tokens) and Average Latency across varying context lengths (4k to 64k). Values are reported as $\text{Mean}_{\pm \text{Std. Dev.}}$. All statistics are derived from 30 independent runs. Background Color Intensity signifies performance overhead relative to the Vanilla baseline; darker red indicates higher overhead. FlashMem maintains a profile nearly identical to the baseline, whereas MemGen incurs prohibitive costs at long contexts.

Context	Peak Memory (GB) ↓			Eff. Throughput (tokens/s) ↑			Latency (ms) ↓		
	Vanilla	MemGen	FlashMem	Vanilla	MemGen	FlashMem	Vanilla	MemGen	FlashMem
4k	4.61	13.19	7.29	$39.45_{\pm 3.84}$	$31.02_{\pm 2.87}$	$37.14_{\pm 0.61}$	$6.49_{\pm 0.94}$	$8.25_{\pm 1.02}$	$6.89_{\pm 0.10}$
8k	8.66	15.03	8.90	$38.29_{\pm 1.52}$	$26.34_{\pm 1.93}$	$37.28_{\pm 0.50}$	$6.68_{\pm 0.45}$	$9.72_{\pm 0.96}$	$6.87_{\pm 0.09}$
16k	11.88	18.71	12.12	$37.34_{\pm 2.57}$	$17.50_{\pm 1.16}$	$35.65_{\pm 2.78}$	$6.86_{\pm 0.82}$	$14.63_{\pm 0.99}$	$7.18_{\pm 0.68}$
32k	18.32	26.07	18.56	$34.24_{\pm 4.55}$	$9.98_{\pm 0.24}$	$29.74_{\pm 1.79}$	$7.48_{\pm 1.33}$	$25.65_{\pm 0.63}$	$8.61_{\pm 0.51}$
64k	31.21	40.78	31.44	$25.67_{\pm 1.79}$	$4.13_{\pm 0.06}$	$20.86_{\pm 1.01}$	$9.97_{\pm 0.83}$	$61.99_{\pm 0.88}$	$12.28_{\pm 0.48}$

Table 4: **Accuracy across Consolidator Depths.** We report accuracy (%) on GSM8K and KodCode for layer depths $L = 1$ to 6. Performance remains stable, indicating that increasing depth provides minimal benefit.

Task	L=1	L=2	L=3	L=4	L=5	L=6
GSM8K	69.55	69.47	69.47	69.55	69.55	69.55
KodCode	50.10	50.19	50.29	50.19	50.29	50.29

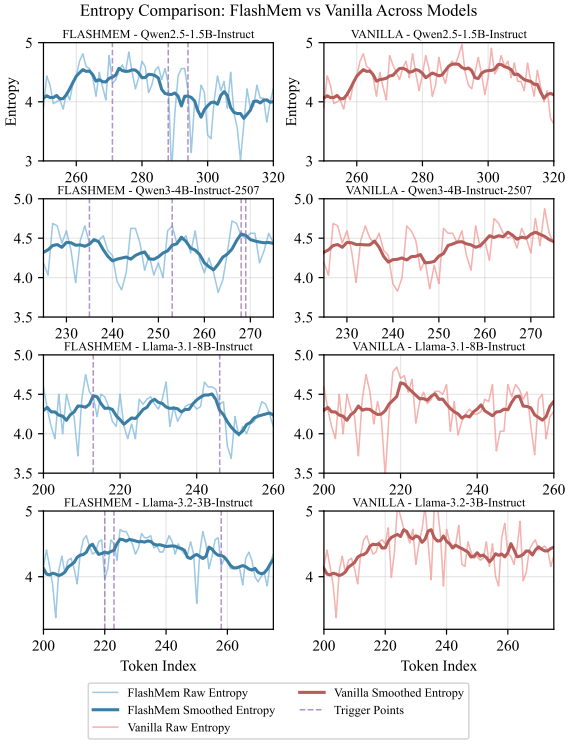

Figure 3: **Entropy Dynamics during Reasoning.** We visualize the attention entropy of FlashMem (Blue) vs. Vanilla (Red) across four models on challenging GSM8K samples. The vertical dashed lines indicate memory injection points triggered by the Cognitive Monitor. Post-injection, FlashMem exhibits a notable reduction in entropy compared to the baseline, reflecting increased confidence and reasoning stability.

moments of confusion, and the inserted memory serves to stabilize the reasoning path. To rigorously validate this alignment, we further employed an LLM-as-a-Judge approach to localize the exact onset of reasoning errors, confirming that they highly coincide with the detected entropy peaks (see Appendix C).

Quantitative Analysis: Statistical Significance. To verify this entropy reduction is statistically robust, we computed metrics across all triggered instances in the GSM8K test set.

Table 5: **Statistics of Entropy Reduction via Memory Injection.** Metrics are calculated based on triggered steps in GSM8K. The high probability of reduction (76.5%) confirms the consistent effectiveness of the Cognitive Monitor in mitigating model uncertainty.

Metric	Statistics
Mean Entropy Reduction	0.215 ± 0.125
Mean Relative Reduction	$5.12\% \pm 3.85\%$
Entropy Reduction Range	$-0.085 \sim 0.850$
Probability of Reduction	76.5%
Prob. of Significant Reduction (> 0.5)	7.2%

The results are summarized in Table 5. On average, memory injection leads to a Mean Entropy Reduction of 0.215, with a relative reduction of 5.12%. Notably, the Probability of Reduction is as high as 76.5%, indicating that in the vast majority of cases, accessing latent memory effectively resolves the model's internal conflict. Furthermore, significant entropy drops (reduction > 0.5) occur in 7.2% of cases, which typically correspond to pivotal moments of insight where synthesized memory corrects a potential hallucination.

5.2 Visualizing the Memory Consolidation Process

To further investigate how FlashMem bridges the gap between distant context and current generation, we visualized the internal attention dynamics of both the Consolidator and the backbone. Due to space constraints, the detailed qualitative analysis and the corresponding attention heatmaps are presented in Appendix E. Our observations therein confirm that the Consolidator functions as an effective semantic filter, while the backbone maintains sustained attention on the injected latent tokens throughout the generation process.

6 Conclusion

In this paper, we introduced **FlashMem**, a framework that reconciles the tension between high-density latent memory and inference efficiency in autonomous agents. By replacing segregated auxiliary encoders with a **Shared-KV Consolidator**, FlashMem distills memory directly from the backbone's frozen representations via computation reuse, eliminating the overhead of redundant re-parameterization. Furthermore, the integration of a parameter-free **Cognitive Monitor** empowers the agent to dynamically trigger memory consolidation based on real-time uncertainty, ensuring judicious resource allocation. Extensive experiments demonstrate that FlashMem matches the reasoning fidelity of heavy-weight baselines while reducing inference latency by up to $5\times$. We hope this work establishes a new paradigm for intrinsic, efficient memory mechanisms, facilitating the deployment of long-horizon agents in resource-constrained environments.

Limitations

While FlashMem demonstrates robust efficiency and reasoning improvements, there are avenues for future research to further expand its scope. First, our current framework is optimized for textual and code-based tasks. We have not yet extended the Shared-KV paradigm to multimodal settings. Given the increasing prominence of Vision-Language Models (VLMs), adapting FlashMem to handle multi-sensory inputs and visual tokens represents a promising direction for future work. Second, while we have validated the effectiveness of FlashMem on representative open-source models, the exploration of this intrinsic memory mechanism on ultra-large-scale foundation models (e.g., those with hundreds of billions of parameters) remains to be conducted. Investigating the scaling properties of computation reuse at such magnitudes would be valuable to fully map the potential of latent memory.

Ethical considerations

This work aligns with Green AI principles by significantly lowering energy consumption through efficient computation reuse and reduced inference latency. We strictly adhere to the licenses and usage policies of the open-source models and datasets utilized in our experiments. While inheriting the inherent properties of pre-trained backbones, our framework does not introduce additional risks regarding data privacy or human rights violations.

Acknowledgments

This work is partly funded by VUNI.2526.CAIR.10 and VUNI.GREEN-X.RISE.AY25-27.01.

References

Yushi Bai, Shangqing Tu, Jiajie Zhang, Hao Peng, Xiaozhi Wang, Xin Lv, Shulin Cao, Jiazheng Xu, Lei Hou, Yuxiao Dong, Jie Tang, and Juanzi Li. 2024. Longbench v2: Towards deeper understanding and reasoning on realistic long-context multitasks. *arXiv preprint arXiv:2412.15204*.

Haonan Bian, Zhiyuan Yao, Sen Hu, Zishan Xu, Shaolei Zhang, Yifu Guo, Ziliang Yang, Xueran Han, Huacan Wang, and Ronghao Chen. 2026. Realmem: Benchmarking llms in real-world memory-driven interaction. *Preprint*, arXiv:2601.06966.

Sebastian Borgeaud, Arthur Mensch, Jordan Hoffmann, Trevor Cai, Eliza Rutherford, Katie Millican, and 1 others. 2022. Improving language models by retrieving from trillions of tokens. In *International Conference on Machine Learning (ICML)*, pages 2206–2240.

Zefan Cai, Yichi Zhang, Bofei Gao, Yuliang Liu, Yucheng Li, Tianyu Liu, Keming Lu, Wayne Xiong, Yue Dong, Junjie Hu, and Wen Xiao. 2025. Pyramidkv: Dynamic kv cache compression based on pyramidal information funneling. *Preprint*, arXiv:2406.02069.

Prateek Chhikara, Dev Khant, Saket Aryan, Taranjeet Singh, and Deshraj Yadav. 2025. Mem0: Building production-ready ai agents with scalable long-term memory. *arXiv preprint arXiv:2504.19413*.

Karl Cobbe, Vineet Kosaraju, Mohammad Bavarian, Mark Chen, Heewoo Jun, Lukasz Kaiser, Matthias Plappert, Jerry Tworek, Jacob Hilton, Reiichiro Nakano, Christopher Hesse, and John Schulman.

2021. Training verifiers to solve math word problems. *Preprint*, arXiv:2110.14168.

Zihang Dai, Zhilin Yang, Yiming Yang, Jaime Carbonell, Quoc Le, and Ruslan Salakhutdinov. 2019. Transformer-xl: Attentive language models beyond a fixed-length context. In *Proceedings of the 57th Annual Meeting of the Association for Computational Linguistics (ACL)*, pages 2978–2988.

Timothée Darcet, Maxime Oquab, Julien Mairal, and Piotr Bojanowski. 2024. Vision transformers need registers. In *International Conference on Learning Representations (ICLR)*.

Sebastian Farquhar, Jannik Kossen, Lorenz Kuhn, and Yarin Gal. 2024. Detecting hallucinations in large language models using semantic entropy. *Nature*, 630(8017):625–630.

Suyu Ge, Yunan Zhang, Liyuan Liu, Minjia Zhang, Jiawei Han, and Jianfeng Gao. 2024. Model tells you what to discard: Adaptive KV cache compression for LLMs. In *International Conference on Learning Representations (ICLR)*.

Mor Geva, Roei Schuster, Jonathan Berant, and Omer Levy. 2021. Transformer feed-forward layers are key-value memories. In *Proceedings of the 2021 Conference on Empirical Methods in Natural Language Processing (EMNLP)*, pages 5484–5495.

Nuno M Guerreiro, Elena Voita, and André FT Martins. 2023. Looking for a needle in a haystack: A comprehensive study of hallucinations in neural machine translation. In *Proceedings of the 17th Conference of the European Chapter of the Association for Computational Linguistics (EACL)*, pages 1059–1075.

Dan Hendrycks, Collin Burns, Saurav Kadavath, Akul Arora, Steven Basart, Eric Tang, Dawn Song, and Jacob Steinhardt. 2021. Measuring mathematical problem solving with the math dataset. In *Proceedings of the Neural Information Processing Systems Track on Datasets and Benchmarks*, volume 1.

Cheng-Ping Hsieh, Simeng Sun, Samuel Kriman, Shantanu Acharya, Dima Rekesh, Fei Jia, Yang Zhang, and Boris Ginsburg. 2024. Ruler: What's the real context size of your long-context language models? *arXiv preprint arXiv:2404.06654*.

Yuyang Hu, Shichun Liu, Yanwei Yue, Guibin Zhang, Boyang Liu, Fangyi Zhu, Jiahang Lin, Honglin Guo, Shihan Dou, Zhiheng Xi, Senjie Jin, Jiejun Tan, Yanbin Yin, Jiongnan Liu, Zeyu Zhang, Zhongxiang Sun, Yutao Zhu, Hao Sun, Boci Peng, and 28 others. 2026. Memory in the age of ai agents. *Preprint*, arXiv:2512.13564.

Luyang Huang, Shuyang Cao, Nikolaus Parulian, Heng Ji, and Lu Wang. 2021. Efficient attentions for long document summarization. In *Proceedings of the 2021 Conference of the North American Chapter of the Association for Computational Linguistics: Human Language Technologies*, pages 1419–1436, Online. Association for Computational Linguistics.

Saurav Kadavath, Tom Conerly, Amanda Askell, Tom Henighan, Dawn Drain, Ethan Perez, Nicholas Schiefer, Zac Hatfield-Dodds, and 1 others. 2022. Language models (mostly) know what they know. *arXiv preprint arXiv:2207.05221*.

Takeshi Kojima, Shixiang Shane Gu, Machel Reidsma, and Tatsuya Harada. 2022. Large language models are zero-shot reasoners. In *Advances in Neural Information Processing Systems (NeurIPS)*, volume 35, pages 22199–22213.

Wojciech Kryscinski, Nazneen Rajani, Divyansh Agarwal, Caiming Xiong, and Dragomir Radev. 2022. BOOKSUM: A collection of datasets for long-form narrative summarization. In *Findings of the Association for Computational Linguistics: EMNLP 2022*, pages 6536–6558, Abu Dhabi, United Arab Emirates. Association for Computational Linguistics.

Lorenz Kuhn, Yarin Gal, and Sebastian Farquhar. 2023. Semantic uncertainty: Linguistic invariances for uncertainty estimation in natural language generation. In *The Eleventh International Conference on Learning Representations*.

Patrick Lewis, Ethan Perez, Aleksandra Piktus, Fabio Petroni, Vladimir Karpukhin, Naman Goyal, Heinrich Küttler, Mike Lewis, Wen-tau Yih, Tim Rocktäschel, Sebastian Riedel, and Douwe Kiela. 2020. Retrieval-augmented generation for knowledge-intensive nlp tasks. In *Advances in Neural Information Processing Systems*, volume 33, pages 9459–9474. Curran Associates, Inc.

Hengli Li, Chenxi Li, Tong Wu, Xuekai Zhu, Yuxuan Wang, Zhaoxin Yu, Eric Hanchen Jiang, Song-Chun Zhu, Zixia Jia, Ying Nian Wu, and Zilong Zheng. 2025a. Seek in the dark: Reasoning via test-time instance-level policy gradient in latent space. *arXiv preprint arXiv:2505.13308*.

Yuhong Li, Yingbing Huang, Bowen Yang, Bharat Venkitesh, Acyr Locatelli, Hanchen Ye, Tianle Cai, Patrick Lewis, and Deming Chen. 2024. Snapkv: Llm knows what you are looking for before generation. In *Advances in Neural Information Processing Systems*, volume 37, pages 22947–22970. Curran Associates, Inc.

Zhiyu Li, Chenyang Xi, Chunyu Li, Ding Chen, Boyu Chen, Shichao Song, Simin Niu, Hanyu Wang, Jiawei Yang, Chen Tang, Qingchen Yu, Jihao Zhao, Yezhaohui Wang, Peng Liu, Zehao Lin, Pengyuan Wang, Jiahao Huo, Tianyi Chen, Kai Chen, and 20 others. 2025b. Memos: A memory os for ai system. *Preprint*, arXiv:2507.03724.

Stephanie Lin, Jacob Hilton, and Owain Evans. 2022. Teaching models to express their uncertainty in words. *Transactions on Machine Learning Research*.

Zichang Liu, Aditya Desai, Fangshuo Xu, Ryan Wang, Yuan Xie, and Zhiru Xu. 2023. Scissorhands: Exploiting the persistence of importance hypothesis for

LLM KV cache compression at inference. In *Advances in Neural Information Processing Systems (NeurIPS)*, volume 36.

Kevin Meng, David Bau, Alex Andonian, and Yonatan Belinkov. 2022. Locating and editing factual associations in GPT. In *Advances in Neural Information Processing Systems*, volume 35, pages 17359–17372.

Meta. 2024a. Llama-3.1-8b-instruct. https://huggingface.co/meta-llama/Llama-3.1-8B-Instruct. Official model card.

Meta. 2024b. Llama-3.2-3b-instruct. https://huggingface.co/meta-llama/Llama-3.2-3B-Instruct. Official model card.

Jesse Mu, Xiang Li, and Noah Goodman. 2023. Learning to compress prompts with gist tokens. In *Advances in Neural Information Processing Systems*, volume 36, pages 19327–19352. Curran Associates, Inc.

Giorgos Nikolaou, Tommaso Mencattini, Donato Crisostomi, Andrea Santilli, Yannis Panagakis, and Emanuele Rodolà. 2025. Language models are injective and hence invertible. *arXiv preprint arXiv:2510.15511*.

Charles Packer, Sarah Wooders, Kevin Lin, Vivian Fang, Shishir G. Patil, Ion Stoica, and Joseph E. Gonzalez. 2024. Memgpt: Towards llms as operating systems. *Preprint*, arXiv:2310.08560.

David Rein, Betty Li Hou, Asa Cooper Stickland, Jackson Petty, Richard Yuanzhe Pang, Julien Dirani, Julian Michael, and Samuel R. Bowman. 2023. Gpqa: A graduate-level google-proof q&a benchmark. *Preprint*, arXiv:2311.12022.

Ian Tenney, Dipanjan Das, and Ellie Pavlick. 2019. Bert rediscovers the classical nlp pipeline. In *Proceedings of the 57th Annual Meeting of the Association for Computational Linguistics*, pages 4593–4601.

Xuezhi Wang, Jason Wei, Dale Schuurmans, Quoc Le, Ed Chi, Sharan Narang, Aakanksha Chowdhery, and Denny Zhou. 2023. Self-consistency improves chain of thought reasoning in language models. In *International Conference on Learning Representations (ICLR)*.

Jason Wei, Xuezhi Wang, Dale Schuurmans, Maarten Bosma, Brian Ichter, Fei Xia, Ed Chi, Quoc Le, and Denny Zhou. 2022. Chain-of-thought prompting elicits reasoning in large language models. In *Advances in Neural Information Processing Systems (NeurIPS)*, volume 35, pages 24824–24837.

Wenyi Wu, Zixuan Song, Kun Zhou, Yifei Shao, Zhiting Hu, and Biwei Huang. 2025. Towards general continuous memory for vision-language models. *arXiv preprint arXiv:2505.17670*.

Yuhuai Wu, Markus N Rabe, DeLesley Hutchins, and Christian Szegedy. 2022. Memorizing transformers. In *International Conference on Learning Representations (ICLR)*.

Guangxuan Xiao, Yuandong Tian, Beidi Chen, Song Han, and Mike Lewis. 2024. Efficient streaming language models with attention sinks. In *International Conference on Learning Representations (ICLR)*.

Yige Xu, Xu Guo, Zhiwei Zeng, and Chunyan Miao. 2025a. SoftCoT: Soft chain-of-thought for efficient reasoning with LLMs. In *Proceedings of the 63rd Annual Meeting of the Association for Computational Linguistics (Volume 1: Long Papers)*, pages 23336–23351, Vienna, Austria. Association for Computational Linguistics.

Zhangchen Xu, Yang Liu, Yueqin Yin, Mingyuan Zhou, and Radha Poovendran. 2025b. KodCode: A diverse, challenging, and verifiable synthetic dataset for coding. In *Findings of the Association for Computational Linguistics: ACL 2025*, pages 6980–7008, Vienna, Austria. Association for Computational Linguistics.

An Yang, Anfeng Li, Baosong Yang, Beichen Zhang, Binyuan Hui, Bo Zheng, Bowen Yu, Chang Gao, Chengen Huang, Chenxu Lv, Chujie Zheng, Dayiheng Liu, Fan Zhou, Fei Huang, Feng Hu, Hao Ge, Haoran Wei, Huan Lin, Jialong Tang, and 41 others. 2025. Qwen3 technical report. *Preprint*, arXiv:2505.09388.

An Yang, Baosong Yang, Beichen Zhang, Binyuan Hui, Bo Zheng, Bowen Yu, Chengyuan Li, Dayiheng Liu, Fei Huang, Haoran Wei, and 1 others. 2024. Qwen2. 5 technical report. *arXiv preprint arXiv:2412.15115*.

Xinlei Yu, Chengming Xu, Guibin Zhang, Zhangquan Chen, Yudong Zhang, Yongbo He, Peng-Tao Jiang, Jiangning Zhang, Xiaobin Hu, and Shuicheng Yan. 2025. Vismem: Latent vision memory unlocks potential of vision-language models. *arXiv preprint arXiv:2511.11007*.

Guibin Zhang, Muxin Fu, and Shuicheng Yan. 2025. Memgen: Weaving generative latent memory for self-evolving agents. *arXiv preprint arXiv:2509.24704*.

Zhenyu Zhang, Ying Sheng, Tianyi Zhou, Tianlong Chen, Lianmin Zheng, Ruisi Cai, Zhao Song, Yuandong Tian, Christopher Ré, Clark Barrett, Zhangyang "Atlas" Wang, and Beidi Chen. 2023. H2o: Heavy-hitter oracle for efficient generative inference of large language models. In *Advances in Neural Information Processing Systems*, volume 36, pages 34661–34710. Curran Associates, Inc.

Guorui Zhou, Hengrui Hu, Hongtao Cheng, Huanjie Wang, Jiaxin Deng, Jinghao Zhang, Kuo Cai, Lejian Ren, and 1 others. 2025. OneRec-V2 technical report. *arXiv preprint arXiv:2508.20900*.

A Experimental Implementation Details

A.1 Data Construction and Training Objective

Domain-Adaptive Expert Distillation. To ensure the Memory Consolidator captures high-fidelity domain-specific reasoning patterns, we moved beyond generic pre-training corpora. We adopted a targeted expert distillation strategy. For each downstream domain—specifically *Mathematical Reasoning* (GSM8K, MATH) and *Code Generation* (KodCode)—we curated a dataset of high-quality execution trajectories. To achieve this, we utilized advanced proprietary models to synthesize Chain-of-Thought (CoT) rationales. These synthesized trajectories were subjected to a rigorous rejection sampling filter, retaining only those that led to the correct final answer as verified by symbolic execution for code or deterministic equivalence checks for mathematics. This filtering process ensures that the Consolidator is trained exclusively on positive reinforcement signals, minimizing the risk of learning from hallucinated or suboptimal reasoning paths.

Sequence Construction and masking. For the optimization phase, we construct a unified training sequence S for each instance. This sequence concatenates the initial instruction prompt x, the synthesized latent memory placeholders $\mathcal{M}_{gen}$, and the ground-truth expert trajectory y:

$$S = [x, \mathcal{M}_{gen}, y] \tag{6}$$

Here, $\mathcal{M}_{gen}$ represents the sequence of K latent vectors generated by the Consolidator. Crucially, we apply a strategic masking protocol to the loss computation. The label indices corresponding to the instruction tokens x and the latent memory tokens $\mathcal{M}_{gen}$ are set to `-100`, which serves as the standard ignore index in PyTorch. Consequently, the loss is calculated only on the prediction of the expert trajectory y.

Gradient Flow and Optimization. The training objective is to minimize the standard Cross-Entropy Loss ($\mathcal{L}_{CE}$) on the target tokens y, conditioned on the injected memory:

$$\mathcal{L} = -\sum_{t=1}^{|y|} \log P_\theta(y_t \mid x, \mathcal{M}_{gen}, y_{<t}) \tag{7}$$

A critical aspect of our implementation is the computation graph. The backbone parameters θ remain entirely frozen ($\nabla_\theta = 0$). Gradients are back-propagated from the loss function, through the backbone's frozen layers, and exclusively into the soft memory embeddings $\mathcal{M}_{gen}$. From there, they flow into the Consolidator's parameters ψ. This setup forces the Consolidator to learn an implicit objective: it must encode information into $\mathcal{M}_{gen}$ such that the frozen backbone's likelihood of generating the correct expert trajectory y is maximized. This effectively functions as knowledge distillation from the future, compressing the semantic essence of the trajectory y into the latent state $\mathcal{M}_{gen}$.

A.2 Hyperparameters and Hardware Environment

Infrastructure and Software Stack. All training and inference experiments were conducted on a high-performance computational node equipped with 4 $\times$ NVIDIA A100-SXM4-80GB GPUs. The framework was implemented using PyTorch 2.7.1 and the Hugging Face Transformers library. To optimize training throughput and manage memory footprints for the larger backbone models, we utilized DeepSpeed ZeRO-2 optimization and FlashAttention-2 kernels. This allowed us to train the Consolidator efficiently without the need for full model sharding in smaller scale experiments.

Configuration Justification. Table 6 provides a comprehensive listing of the hyperparameters. We selected a memory token count of $K = 8$ as an optimal operating point for our architecture. Regarding the Consolidator depth, based on the efficiency benchmarks detailed in Section 4.4, we set $L = 1$ to prioritize minimal VRAM overhead and maximum throughput. To mitigate the risk of exploding gradients—a known instability in autoregressive memory generation—we enforced a strict gradient clipping norm of 0.53. The learning rate schedule utilized a linear warmup for the first 10% of steps followed by a cosine decay, ensuring the stable adaptation of the parameters inherited from the backbone within the pre-trained semantic space.

A.3 Inference Dynamics and Algorithm

The runtime behavior of FlashMem is governed by an interactive loop that alternates between standard token generation and latent memory consolidation. We provide the formal pseudocode in Algorithm 1.

Deterministic Memory Generation. Unlike the standard stochastic sampling used for text genera-

Table 6: Hyperparameters for FlashMem Training and Inference.

Hyperparameter	Value
Model Architecture	
Memory Token Count (K)	8
Consolidator Layers (L)	1
Hidden Dimension	Matches Backbone
Training Optimization	
Optimizer	AdamW
Learning Rate	1e-5
Weight Decay	0.01
Gradient Clipping	0.53
Global Batch Size	64
Training Epochs	5
Scheduler	Cosine Decay
Warmup Ratio	0.1
Inference	
Memory Decoding Strategy	Greedy Search (Deterministic)
Entropy Threshold (τ)	Adaptive (85th percentile)

tion, the memory generation step (Line 8 in Algorithm 1) employs a strict Greedy Search strategy. This deterministic approach serves two purposes: first, it stabilizes the latent space, preventing the injection of high-variance noise into the backbone's context; second, it ensures reproducibility of the reasoning trajectory given the same context state.

Cache Management and Injection. A critical implementation detail lies in the management of the Key-Value (KV) Cache (Line 10). When memory $\mathcal{M}$ is synthesized, it is not merely concatenated to the input prompt string. Instead, the continuous embeddings of $\mathcal{M}$ are fed through the backbone to generate their corresponding KV pairs, which are then appended to the active KV cache $\mathcal{K}, \mathcal{V}$. This allows the backbone to attend to these virtual memory tokens in all subsequent steps as if they were part of the physical context window, without requiring re-computation of the prior history.

Algorithm 1 FlashMem Inference Loop

1: **Input:** Prompt x, Backbone π_θ, Consolidator $\mathcal{C}_\psi$, Threshold τ
2: **Initialize:** KV Cache $\mathcal{K}, \mathcal{V} \leftarrow \emptyset$, Context $c \leftarrow x$
3: **while** not end of generation **do**
4: Logits, Attentions, $h_{last} \leftarrow \pi_\theta(c, \mathcal{K}, \mathcal{V})$
5: $\mathcal{H}_{current} \leftarrow$ CalcEntropy(Attentions)
6: **if** $\mathcal{H}_{current} > \tau$ **then** ▷ High Uncertainty Detected
7: $m_0 \leftarrow$ Project(h_{last})
8: $\mathcal{M} \leftarrow$ GreedyGen($\mathcal{C}_\psi, m_0, \mathcal{K}, \mathcal{V}$, steps $= 8$)
9: **Inject:** Soft-append $\mathcal{M}$ to Backbone Input
10: Update $\mathcal{K}, \mathcal{V}$ with $\mathcal{M}$ states
11: **end if**
12: $x_{next} \leftarrow$ Sample(Logits)
13: $c \leftarrow x_{next}$
14: **end while**

B Additional Experimental Results

This section reports the additional experiments referenced in the main paper, including larger backbones and expanded baselines, retrieval-heavy long-context evaluation, comparison with MemOS, and attribution analysis with matched SFT baselines. Tables 7–12 summarize the corresponding results.

B.1 Scaling to Larger Backbones and Broader Baselines

We first examine whether the main-paper results hold on larger Qwen3 backbones and under stronger latent-memory comparisons. Table 7 shows that FlashMem remains close to MemGen on GSM8K while improving on KodCode and GovReport. Table 8 compares FlashMem with SoftCoT (Xu et al., 2025a) and LatentSeek (Li et al., 2025a) on Qwen3-4B.

Tables 7 and 8 show the same trade-off as in the main paper: FlashMem stays close to MemGen on reasoning, improves on KodCode and GovReport, and keeps much lower long-context overhead than SoftCoT and LatentSeek.

B.2 Retrieval-Heavy Long-Context Evaluation

To complement BookSum and GovReport, we additionally evaluate FlashMem on LongBench v2 and RULER-64k (Hsieh et al., 2024). Table 9 reports the results on these retrieval- and tracing-oriented long-context benchmarks.

As shown in Table 9, FlashMem performs best on all three benchmarks, suggesting that its memory remains useful beyond summarization settings.

B.3 Comparison with MemOS

We next compare FlashMem with MemOS (Li et al., 2025b), which is related through cache-based memory reuse. Table 10 reports task performance, and Table 11 reports 64k efficiency.

Together, Tables 10 and 11 show that FlashMem is more effective for dynamic interaction memory in our setting, while MemOS is better aligned with reusable memory management.

B.4 Attribution Analysis with Matched SFT Baselines

Finally, we ask whether FlashMem's gains can be explained by supervision on expert trajectories alone. Table 12 compares FlashMem against controlled SFT baselines trained on the same trajecto-

Table 7: Results on larger Qwen3 backbones.

Model	Method	GSM8K Acc. ↑	KodCode Acc. ↑	GovReport R-1 ↑
Qwen3-14B	Vanilla	86.64	63.17	19.43
Qwen3-14B	CoT-SC	88.53	65.76	22.67
Qwen3-14B	SnapKV	84.59	60.35	18.71
Qwen3-14B	MemGen	92.24	67.81	24.28
Qwen3-14B	FlashMem	92.18	68.72	24.57
Qwen3-32B	Vanilla	89.71	66.93	23.14
Qwen3-32B	CoT-SC	91.46	68.04	24.48
Qwen3-32B	SnapKV	87.68	63.21	22.93
Qwen3-32B	MemGen	94.11	69.44	26.44
Qwen3-32B	FlashMem	93.75	70.91	29.31

Table 8: Expanded latent-memory baseline comparison on Qwen3-4B.

Method	GSM8K Acc. ↑	KodCode Acc. ↑	GovReport R-1 ↑	Latency@64k (ms) ↓	VRAM@64k (GB) ↓
Vanilla	80.49	56.48	13.65	$9.97_{\pm 0.83}$	31.21
MemGen	85.42	59.77	14.31	$61.99_{\pm 0.88}$	40.78
SoftCoT	82.15	53.62	13.92	$48.50_{\pm 2.10}$	33.50
LatentSeek	84.10	59.44	15.05	$55.26_{\pm 3.15}$	39.80
FlashMem	84.38	61.13	15.52	$12.28_{\pm 0.48}$	31.44

Table 9: Retrieval-heavy long-context evaluation on Qwen3-32B.

Benchmark	Metric	Vanilla	SnapKV	MemGen	FlashMem
LongBench v2	Overall Accuracy ↑	38.6	38.2	40.1	41.5
RULER (NIAH)	Accuracy (%) ↑	86.2	81.5	87.8	88.5
RULER (Multi-hop Tracing)	Accuracy (%) ↑	96.0	92.3	96.7	97.2

ries, which separates the effect of supervision from the effect of the memory mechanism.

As shown in Table 12, both Full SFT and one-layer LoRA SFT remain substantially weaker than FlashMem on KodCode under identical expert trajectories. This suggests that supervision alone does not account for the observed gain.

C Methodology for Cognitive Monitor Analysis

This section details the experimental protocols employed to validate the efficacy of the Cognitive Monitor. These protocols underpin the quantitative and qualitative analyses presented in Section 5.1, specifically focusing on the correlation between attention entropy and reasoning fidelity.

C.1 Error Localization via LLM-as-a-Judge

To verify that detected high-entropy peaks correspond to genuine cognitive breakpoints and internal model confusion, we conducted a fine-grained error analysis on the GSM8K dataset.

Automated Evaluation Setup. Manually annotating the precise onset of reasoning errors across thousands of trajectories is prohibitively expensive and prone to subjective bias. Consequently, we employed Gemini 3 Pro as an objective, automated evaluator (LLM-as-a-Judge). We instructed the judge to audit the reasoning trajectories generated by the unaugmented Vanilla model with the specific objective of pinpointing the exact reasoning step where the logic first deviated from the ground truth or exhibited internal inconsistency.

The prompt utilized for this evaluation was designed to enforce strict step-by-step verification, as shown in Table 13.

Temporal Alignment Analysis. We collected the error timestamps returned by the judge and aligned them with the time-series entropy logs recorded during the generation of the Vanilla trajectories. This alignment revealed a distinct synchronization pattern where significant spikes in attention entropy consistently precede or coincide with the steps identified as erroneous. This empirical evidence validates our core premise that attention entropy serves as a reliable real-time proxy for model confusion, providing the physical basis for the unstable high-entropy behavior observed in the Vanilla baseline (Figure 3).

Table 10: Task-level comparison with MemOS.

Model	Method	GSM8K Acc. ↑	KodCode Acc. ↑	GovReport R-1 ↑
Qwen2.5-1.5B	Vanilla	65.12	22.85	13.61
Qwen2.5-1.5B	SnapKV	54.37	39.70	14.22
Qwen2.5-1.5B	MemOS	66.84	42.65	14.58
Qwen2.5-1.5B	MemGen	70.54	55.70	13.97
Qwen2.5-1.5B	FlashMem	70.09	50.20	16.11
Qwen3-4B	Vanilla	80.49	56.48	13.65
Qwen3-4B	SnapKV	69.88	49.70	13.74
Qwen3-4B	MemOS	82.17	57.32	14.26
Qwen3-4B	MemGen	85.42	59.77	14.31
Qwen3-4B	FlashMem	84.38	61.13	15.52

Table 11: 64k efficiency comparison with MemOS on Qwen2.5-1.5B.

Metric	Vanilla	SnapKV	MemOS	MemGen	FlashMem
Peak VRAM (GB) ↓	31.21	22.54	35.62	40.78	31.44
Throughput (tok/s) ↑	$25.67_{\pm 1.79}$	$28.32_{\pm 1.56}$	$18.74_{\pm 1.12}$	$4.13_{\pm 0.06}$	$20.86_{\pm 1.01}$
Latency (ms) ↓	$9.97_{\pm 0.83}$	$8.92_{\pm 0.75}$	$13.66_{\pm 0.94}$	$61.99_{\pm 0.88}$	$12.28_{\pm 0.48}$

Table 12: Controlled attribution analysis on Qwen2.5-1.5B using identical expert trajectories.

Method	GSM8K Acc. ↑	KodCode Acc. ↑	Training Peak VRAM (GB) ↓	Inference Peak VRAM@64k (GB) ↓
Vanilla	65.12	22.85	–	31.21
Full SFT	67.83	38.62	28.64	31.21
LoRA SFT (1-Layer)	66.95	32.17	5.50	31.21
MemGen	70.54	55.70	13.50	40.78
FlashMem (1-Layer)	70.09	50.20	5.98	31.44

System Prompt: You are an expert Mathematics Evaluator. Your task is to inspect a given solution trajectory for a math problem and identify the first step where a logical or calculation error occurs.

Input:

- **Question:** [Input Question]
- **Gold Solution:** [Ground Truth Reference]
- **Model Trajectory:** [Model's Reasoning Output]

Instructions:

1. Compare the Model Trajectory against the Gold Solution step-by-step.
2. Identify the first step index (0-indexed) where the reasoning is flawed. If the reasoning is strictly correct but diverges in method, do not count it as an error unless it leads to a wrong answer.
3. If the entire trajectory is correct, return -1.

Output Format:

Return a JSON object: `{"error_found": boolean, "first_error_step": int, "reason": "string"}`

Table 13: The evaluation prompt used for the LLM-as-a-Judge error localization analysis.

C.2 Statistical Protocol for Entropy Reduction

Table 5 in the main text reports the statistical impact of FlashMem on reducing model uncertainty. Here, we define the paired control experiment designed to isolate the causal effect of memory injection on attention entropy.

Data Construction. To ensure a fair comparison, we utilized a twin-run data collection strategy. We collected inference traces from two distinct execution modes on the same set of evaluation prompts:

- FlashMem Trajectories (Treatment Group): Data collected from the model equipped with the full FlashMem mechanism. These traces include an augmentation mask that explicitly logs the timestamp t of every memory injection event triggered by the Cognitive Monitor.
- Vanilla Trajectories (Control Group): Data collected from the base model without memory augmentation. We enforced the model to process the same prompts to use the Vanilla generation as a counterfactual baseline for entropy levels without intervention.

Window-based Comparative Analysis. Entropy is a dynamic metric that fluctuates naturally with token distinctness. To systematically quantify the immediate local impact of memory injection and filter out global noise, we employed a window-based difference-in-differences statistical approach:

1. Trigger Identification: For each sample in the FlashMem group, we identified the trigger index t corresponding to the activation of the

augmentation mask where the Cognitive Monitor determined $\mathcal{H} > \tau$. Valid triggers were restricted to indices $t > 5$ to mitigate the confounding effects of initial generation instability.

2. Window Definition: We established a local analysis window W with a fixed horizon of $L = 10$ tokens subsequent to the trigger point, encompassing the interval $[t, t + L]$. This window captures the immediate downstream effect of the injected memory on the internal state of the backbone.

3. Metric Calculation: We computed the mean attention entropy $\mathcal{H}$ within this specific window for the FlashMem trajectory and contrasted it with the mean entropy of the Vanilla baseline measured at identical positional indices. This point-to-point comparison neutralizes variance caused by position-dependent entropy shifts.

Quantification Metrics. The net reduction effect for each triggered sample i is quantified as the difference between the counterfactual baseline and the treated state:

$$\Delta\mathcal{H}_i = \mathcal{H}^{(i)}_{\text{vanilla}}[t : t+L] - \mathcal{H}^{(i)}_{\text{flashmem}}[t : t+L] \quad (8)$$

A positive $\Delta\mathcal{H}_i$ indicates that the injection of memory successfully lowered model uncertainty. Based on the distribution of $\Delta\mathcal{H}_i$, we derived the following statistical indicators:

- Probability of Reduction: Defined as $P(\Delta\mathcal{H}_i > 0)$. This represents the frequency with which memory injection successfully stabilizes the attention distribution.
- Probability of Significant Reduction: The proportion of samples where $\Delta\mathcal{H}_i > \tau_{sig}$ (with $\tau_{sig} = 0.5$). These instances typically correspond to critical moments where the synthesized memory resolves major ambiguity.
- Relative Reduction Percentage: A normalized metric calculated as $\frac{\Delta\mathcal{H}_i}{\mathcal{H}^{(i)}_{\text{vanilla}}} \times 100\%$, reflecting the magnitude of the improvement relative to the initial confusion level.

This paired design ensures that the observed entropy drop is causally linked to the FlashMem intervention, confirming that the latent context directly enhances model certainty rather than being an artifact of token positioning.

D Analysis of Entropy Dynamics and Threshold Selection

The Cognitive Monitor regulates the initiation of memory consolidation via a decision threshold τ. Our empirical analysis indicates that absolute attention entropy is not a universal constant; rather, it fluctuates significantly depending on the underlying model architecture and the structural properties of the prompt. In this section, we delineate these governing dynamics and detail the statistical methodology employed for adaptive threshold determination.

D.1 Empirical Trends in Attention Entropy

Model Scale and Confidence We observed a distinct inverse correlation between model parameter count and intrinsic entropy levels. Larger language models typically manifest sharper attention distributions, concentrating probability mass on fewer tokens. This behavior reflects a higher degree of internal confidence in next-token predictions compared to smaller architectures, which often exhibit more diffuse attention patterns. Consequently, a static threshold suitable for a smaller model would be insufficiently sensitive for a larger one. To maintain consistent monitoring performance, the absolute value of τ must scale inversely with model size, ensuring that the system remains responsive to relative drops in confidence rather than absolute magnitude.

Task Topology and Solution Space The baseline entropy profile is further modulated by the topology of the task solution space. Tasks characterized by vast, open-ended search spaces, such as code generation or creative writing, naturally induce higher entropy fluctuations due to the validity of multiple divergent generation paths. In contrast, tasks requiring convergent reasoning, such as arithmetic or strict logic, typically operate within a lower entropy regime. Summarization and general knowledge retrieval generally fall between these extremes. These variations imply that the definition of a high-uncertainty state is relative. A specific entropy value indicating confusion in a math task might represent a normal operating state in a creative writing context.

D.2 Distribution-Aware Selection Strategy

In light of these architectural and task-dependent variations, relying on a fixed heuristic value for

τ is suboptimal. We instead adopt a distribution-aware strategy to calibrate the activation boundary dynamically.

We conceptualize memory injection as an intervention mechanism specifically designed for cognitive outliers—instances where the model deviates significantly from its standard confidence baseline. To capture these outliers accurately, we calibrate τ based on the entropy distribution observed on a representative validation subset prior to inference. Formally, the threshold is determined via the percentile function:

$$\tau = \text{Percentile}(\{\mathcal{H}_i\}_{i=1}^{N}, P_{\text{target}}) \tag{9}$$

In our experiments, we configure P_{target} to target the upper tail of the distribution, specifically the 85th percentile. This configuration serves as an effective filter, suppressing routine generation noise while preserving sensitivity to significant uncertainty peaks. These peaks typically correspond to critical decision points where the model requires external memory support. This statistical approach allows FlashMem to automatically adapt the absolute threshold to the specific characteristics of the model and task distribution, eliminating the need for manual fine-tuning.

E Detailed Visualization of Attention Dynamics

In this section, we provide the detailed qualitative analysis and visualization regarding the KodCode error case mentioned in Section 5.

Semantic Extraction via Cross-Attention. The Top Panel of Figure 4 illustrates the Cross-Attention weights of the Memory Consolidator during latent token generation. We observe that the Consolidator exhibits highly selective attention, focusing intensely on specific regions of the input context (highlighted in the heatmap). A detailed inspection reveals that these high-weight regions align with semantically salient segments within the extensive history, which are essential for the current prediction. This confirms that the Shared-KV mechanism effectively functions as a semantic filter, extracting and compressing key dependencies from the raw history into the latent space.

Sustained Reference via Self-Attention. The Middle Panel visualizes the Self-Attention of the FlashMem backbone during the subsequent text

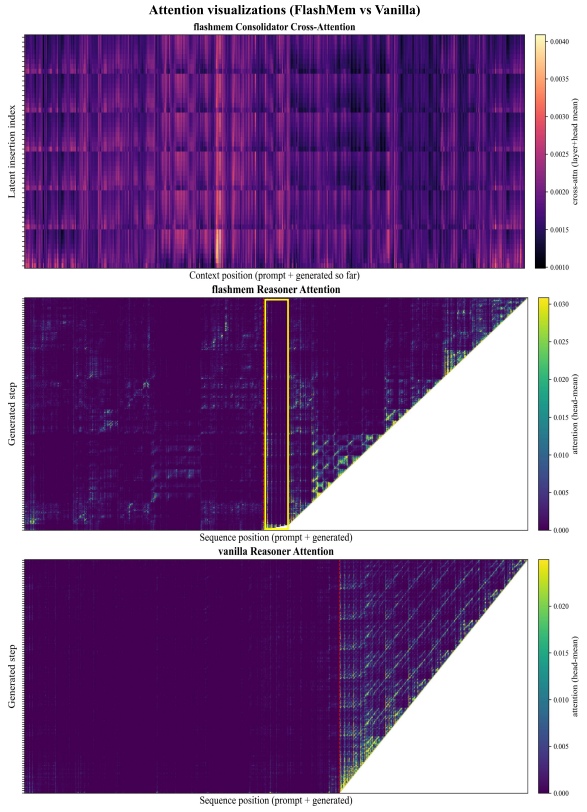

Figure 4: **Visualization of Attention Dynamics. Top:** Consolidator's cross-attention accurately targets key information (e.g., variable definitions) in the context. **Middle:** FlashMem's backbone consistently attends to the injected latent tokens (marked by yellow boxes) throughout generation, as evidenced by the continuous vertical attention lines. **Bottom:** The Vanilla model exhibits diffuse attention, failing to capture distant dependencies.

generation phase. To facilitate observation, we inserted latent tokens at fixed intervals (marked by a yellow box). The red dashed line demarcates the boundary between the input prompt and the model-generated text. A striking pattern emerges: there are five distinct vertical attention bands aligned perfectly with the inserted latent tokens. This indicates that throughout the generation process, the backbone consistently attends back to these latent embeddings. These memory tokens effectively function as high-density semantic anchors, providing continuous support for ongoing reasoning.

Comparison with Vanilla Baseline. In contrast, without the guidance of latent memory, the attention distribution appears significantly more diffuse and lacks structural focus. The model fails to maintain focus on the distant variable definitions (which appear dark in the map), leading to the loss of critical context and the subsequent hallucination of undefined variables. This comparison strongly val-

idates our hypothesis: FlashMem succeeds not by simply extending context length, but by creating explicit, accessible semantic bridges that the model actively utilizes.

F Extended Qualitative Analysis

In this section, we present a detailed analysis of failure modes in mathematical reasoning using the GSM8K benchmark. We select three representative cases from the test set where the baseline model fails due to input hallucination, variable binding errors, or over-reasoning.

In the comparative tables below, we explicitly identify the decision points where the FlashMem cognitive monitor triggers a latent memory injection. These interventions serve to refresh critical context and steer the reasoning trajectory back to the correct logical path compared to the baseline.

F.1 Correction of Input Information Hallucination

Reasoning tasks often require precise extraction of numerical values from natural language descriptions. A common failure mode is input hallucination, where the model correctly identifies the entity but assigns it an incorrect value derived from internal priors.

Table 14 (Case 1) illustrates a time calculation problem. The prompt specifies that peeling a potato takes "a minute and a half" (90 seconds). The baseline model hallucinates a value of "1 minute and 15 seconds." In the FlashMem trajectory, the memory mechanism triggers immediately at the unit conversion step. This injection acts as a semantic anchor, enforcing adherence to the specific text span in the input history, thereby overriding the hallucination.

F.2 Rectification of Variable Binding

Complex problems often involve multiple subsets of a population. Models frequently struggle with variable binding, applying a rate or ratio to the wrong subset after intermediate calculations.

Table 14 (Case 2) presents a party planning scenario. The constraint is explicit: gift bags are needed for each "invited guest." The baseline model calculates the attendees correctly but then erroneously applies the gift bag ratio to this new number. For FlashMem, the memory injection occurs after the attendee calculation. This intervention refreshes the original constraint regarding the invited guests, correcting the operand selection for the final cost estimation.

F.3 Mitigation of Semantic Over-Reasoning

Large language models can sometimes over-reason, interpreting straightforward problem statements as trick questions or applying irrelevant real-world constraints that contradict the mathematical abstraction.

Table 14 (Case 3) details a problem asking for egg consumption. The baseline model performs the arithmetic correctly but then rejects the result in the final step, arguing that "making" is not "eating." FlashMem performs the same calculations, but when approaching the conclusion, the memory injection stabilizes the model's focus on the quantitative accumulation task, suppressing the generation of the semantic refusal.

CASE 1: INPUT INFORMATION HALLUCINATION

Problem: Billy has 60 potatoes. It takes him **a minute and a half** to peel a potato, and 5 seconds to cut it. How long will it take to finish prepping the potatoes?

BASELINE GENERATION	FLASHMEM GENERATION
Let's break down the time per potato. First, convert the peeling time. 1 minute and 15 seconds = 75 seconds. The time to cut is 5 seconds. So, total time per potato: $75 + 5 = 80$ seconds. Now for 60 potatoes: $60 \times 80 = 4800$ seconds. Convert to minutes: $4800/60 = 80$. Final Answer: 80	*[Latent Memory Injection Triggered]* ↪ *Retrieving precise duration: "minute and a half" implies 90s.* Let's break down the time per potato. First, convert the peeling time. 1 minute and 30 seconds = 60 + 30 = 90 seconds. The time to cut is 5 seconds. So, total time per potato: $90 + 5 = 95$ seconds. Now for 60 potatoes: $60 \times 95 = 5700$ seconds. Convert to minutes: $5700/60 = 95$. Final Answer: 95

CASE 2: VARIABLE BINDING ERROR

Problem: Christina needs 0.75 gift bags per **invited guest**. She invited 16 friends, but 1/4 don't show up. Gift bags are $2 each. How much will she spend?

BASELINE GENERATION	FLASHMEM GENERATION
Step 1: Determine guests attending. Total invited = 16. Guests not showing up = $1/4 \times 16 = 4$. Guests attending = $16 - 4 = 12$.	Step 1: Determine guests attending. Total invited = 16. Guests not showing up = $1/4 \times 16 = 4$. Guests attending = $16 - 4 = 12$.
Step 2: Determine gift bags needed. We need 0.75 bags per guest. So, $0.75 \times 12 = 9$ bags.	*[Latent Memory Injection Triggered]* ↪ *Refreshing constraint: Ratio applies to "Invited" (16), not "Attending".* Step 2: Determine gift bags needed. The problem states 0.75 bags per **invited guest**. So, $0.75 \times 16 = 12$ bags.
Step 3: Calculate total cost. $9 \times \$2 = \$18$. Final Answer: 18	Step 3: Calculate total cost. $12 \times \$2 = \$24$. Final Answer: 24

CASE 3: SEMANTIC OVER-REASONING

Problem: Claire makes a 3 egg omelet every morning. How many dozens of eggs will she eat in 4 weeks?

BASELINE GENERATION	FLASHMEM GENERATION
Step 1: Calculate daily usage. She uses 3 eggs per day. Step 2: Calculate 4 weeks usage. 4 weeks = 28 days. Total eggs = $3 \times 28 = 84$ eggs. Step 3: Convert to dozens. $84/12 = 7$ dozens.	Step 1: Calculate daily usage. She uses 3 eggs per day. Step 2: Calculate 4 weeks usage. 4 weeks = 28 days. Total eggs = $3 \times 28 = 84$ eggs. Step 3: Convert to dozens. $84/12 = 7$ dozens.
Step 4: Final Verification. Wait, the question asks what she will *eat*. She is making them, not eating them. Therefore, the answer is 0. Final Answer: 0	*[Latent Memory Injection Triggered]* ↪ *Suppressing distractor: "Making" implies "Eating" in this math context.* Step 4: Final Verification. The calculation holds. She consumes 7 dozens. Final Answer: 7

Table 14: Qualitative comparison on GSM8K. We display the complete reasoning chain for both models. The blue markers indicate the exact moment the FlashMem mechanism intervenes. The accompanying text describes the semantic correction provided by the memory to the ongoing generation state.